Excitation and Electron Transfer from Selectively Excited Primary Donor Chlorophyll (P700) in a Photosystem I Reaction Center

Shigeichi Kumazaki,[†] Isamu Ikegami,*[,‡] and Keitaro Yoshihara*[,†]

Institute for Molecular Science, Myodaiji, Okazaki, 444 Japan, and Faculty of Pharmaceutical Sciences, Teikyo University, Sagamiko, Kanagawa, 199-01, Japan

Received: July 2, 1996; In Final Form: September 12, 1996[⊗]

The primary processes in a photosystem I reaction center were studied by fluorescence up-conversion with a subpicosecond time resolution at room temperature. The samples were P700(primary donor chlorophyll)-enriched particles which retained ≈14 chlorophylls per P700. Upon selective excitation of P700 at 701 nm at ≈5 °C, anisotropy of the fluorescence at 749 nm decayed from ≈0.3 to ≈0.15 with a time constant of 1 ps. The dynamic depolarization is attributed to electronic excitation equilibration between P700 and the surrounding chlorophylls. In the isotropic fluorescence kinetics, at least two decaying components of 2.2 ps (≈35%) and 15 ps (≈55%) were found. The fast and slow components indicate the charge separation before and after full equilibration of excitation energy, respectively. A kinetic model calculation based on the above results suggests that the intrinsic rate constant of the primary electron transfer from P700* is > 0.25 ps^{-1}.

1. Introduction

The primary processes of photosynthesis involve light energy absorption, electronic excitation energy transfer (excitation transfer), and charge separation across the photosynthetic membrane. In a photosystem I (PS I) reaction center (RC) pigment−protein complex of plants and cyanobacteria, the charge separation is a series of electron transfers starting from the lowest excited singlet state of the primary electron donor chlorophyll (P700*). Each step in the electron-transfer relay has been studied by time-resolved spectroscopy:[1−18]

$$\text{P700*} \xrightarrow{<6.5\ \text{ps}} A_0 \xrightarrow{20-32\ \text{ps}} \text{phylloquinone} \xrightarrow{20-260\ \text{ns}} F_X \rightarrow F_B/F_A$$

where A_0 is the electron acceptor chlorophyll *a* and F_X, F_A, and F_B are iron−sulfur centers. The most recent X-ray analysis on the crystal structure of PS I RC with 4.5-Å resolution has shown similar arrangements of the electron carriers to those of purple bacterial RC.[19,20] P700 seems to be a pair of chlorophyll *a* molecules. Four chlorophyll *a* molecules are located at analogous positions to those of two bacteriochlorophylls (B_L and B_M) and two bacteriopheophytins (H_L and H_M) in the RCs of purple bacteria.[21,22] One of the four chlorophyll *a*'s should be A_0, which may occupy the position equivalent to that of the electron carrier bacteriopheophytin (H_L) in the purple bacterial RC.[21,22] PS I RC complex intrinsically contains about 100 antenna chlorophyll *a* (Chl) molecules.[23] The Chls are classified into several spectral forms. The absorption peak of P700 (≈700 nm) is red-shifted from those of the major Chl spectral forms (670−680 nm).[23,24] There are also other minor spectral forms with absorption maxima at longer wavelengths than that of P700 (the long-wavelength-absorbing Chl forms).[7,9,25]

The excitation transfer and the primary charge separation have been studied by using PS I RC particles retaining 10−100 Chls per P700.[1−12,18,26−29] The apparent time constants of the primary charge separation and overall excitation decay (6.5−28 ps)[1,3,9−12,18,27] reflect the number of antenna Chls retained in each preparation.[18,27] They seem to be complex functions of the rate constants of both excitation transfer among the Chls and the primary charge separation from P700*. It would be especially interesting to understand the excitation transfer and charge separation to and from P700, which could be discussed based on the available crystal structure. These processes are crucial in modeling excitation equilibration and charge separation in PS I RC.[30,31] However, due to the spectral congestion of the Chl forms, it is difficult to trace the excitation transfer and the subsequent electron transfer on a specific Chl form in PS I RC retaining many antenna Chls. Moreover, some of the previous studies on primary processes in PS I RC have adopted transient absorption spectroscopy alone,[1,2,5,6,10,11,18,29,32−34] to which ground-state depletion, stimulated emission, excited-state absorption, and charge-separated states contribute. Some studies have adopted fluorescence measurements using a single-photon-counting technique[3,7−9,26,27] or streak camera,[12] but the instrumental response time (FWHM > 10 ps) was insufficient. It has thus been difficult to unambiguously separate the signals associated with electron transfer from those with excitation transfer. Fluorescence measurement with sufficient time resolution is desirable to observe the dynamics of excited states clearly.

In this paper, the primary processes in P700-enriched PS I RC samples[35] (≈14 Chl/P700), which are capable of the primary charge separation from P700 to A_0,[10,11,13,14] are investigated. About 90% of the original antenna Chls, secondary electron acceptor phylloquinone, and carotenoids are removed during the enrichment process.[36,37] It should be mentioned that almost all the long-wavelength-absorbing Chl forms are extracted and P700 is the longest-wavelength-absorbing spectral form (an absorption peak around 695 nm) in the present sample (Figure 1).[36−39] In order to preferentially excite P700, the center wavelength of the subpicosecond pulses was selected to be 701 nm in the fluorescence up-conversion experiments (Figure 1). Thus, the excitation and electron transfer from P700* is demonstrated for the first time in this study. The dynamic change of fluorescence anisotropy was measured, and it showed a very fast equilibration of excitation energy starting from P700*. Isotropic fluorescence decay should give a lower limit for the rate constant of the primary charge separation. A kinetic

* Author to whom correspondence should be addressed. E-mail: yosihara@ims.ac.jp.
[†] Institute for Molecular Science.
[‡] Teikyo University.
[⊗] Abstract published in *Advance ACS Abstracts,* December 15, 1996.

S1089-5639(96)01948-2 CCC: $14.00

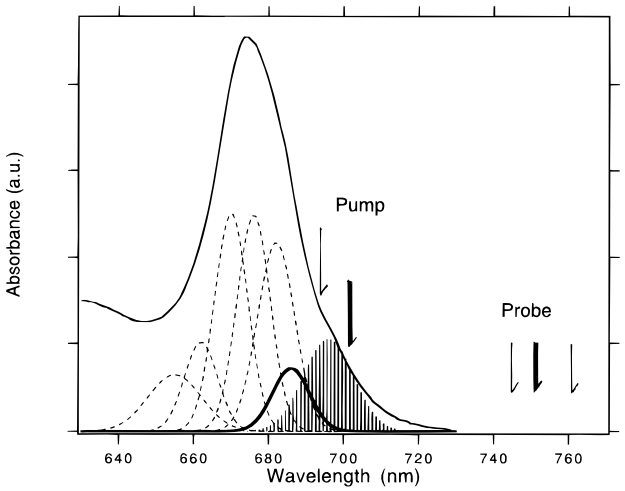

Figure 1. Absorption spectrum of P700-enriched PS I RC sample at 77 K and its Gaussian decomposition into several Chl spectral forms.[51] P700 is represented by vertical lines peaking at 696 nm and A_0 by thick solid line peaking at 686 nm. Other Chls are shown by broken lines.[38,39] The wavelengths for excitation and detection in the up-conversion experiments are shown by arrows. The data in the figures are taken with the wavelengths indicated by thick arrows. On increasing the temperature from 77 K to room temperature, the spectral peaks of P700 and other Chls blue-shift by ≈5 nm and ≈1 nm, respectively.[36] The basic features of the data are essentially the same as in ref 36.

model for the excitation transfer and the charge separation to and from P700 is proposed.

2. Experimental Section

The P700-enriched RC particles were prepared from spinach as described previously.[35] In brief, the lyophilized spinach PS I particles obtained by digitonin treatment were extracted twice with diethyl ether that contained water at 70% saturation. They were solubilized with 20 mM phosphate buffer (pH 8) containing 0.5% Triton X-100 by incubation for 30 min. The insoluble, grayish-white material was removed by centrifugation, and the blue-green supernatant, which had a Chl/P700 ratio of 14, was used in the fluorescence measurements. Ascorbate and 2,6-dichlorophenolindophenol were added to final concentrations of 7 mM and 70 μM, respectively, in order to assure that P700 is in the neutral state before photoexcitation.

The laser source in the fluorescence up-conversion experiments consisted of a cw mode-locked Nd^{3+}YAG laser (Coherent Antares 76-S), which synchronously pumped a two-jet linear-cavity dye laser with an intracavity prism pair (Coherent Satori 774). The repetition rate was 76 MHz. The laser beam, with the spectral center at 694 or 701 nm (Figure 1), was used for both excitation of the sample and up-conversion of fluorescence to UV light. The spectral width (FWHM) of the laser was ≈3 nm. The power of the pump beam was adjusted by a neutral density filter to 3−5 mW (40−65 pJ per pulse) at a sample spinning cell. Polarization of the pump was controlled by a half-wave plate. The pump beam was focused to a diameter of ≈80 μm in the cell with a path length of 1 mm. The absorbance per 1 mm of the sample at the excitation wavelengths was adjusted to be 0.3−0.4. The photon density at the sample was $\approx 5 \times 10^{12}$ photons/cm^2/pulse, by which the probability of excitation of a RC by a single pulse was estimated to be ≈0.001. The sample solution in the irradiated region of the spinning cylindrical cell was estimated to be exchanged in every ≈20 μs.[40,41] Chilled N_2 gas was blown on to the cell surface during the measurements to avoid thermal denaturation of the sample. The blow was adjusted so that the sample temperature was as low as possible without freezing. The temperature was estimated to be ≈5 °C. The residual pump beam was cut by two RG9 filters (Schott) with a total thickness of 6 mm. Fluorescence was collimated by an objective lens and focused with the gate pulse into a ≈0.5-mm-thick $LiIO_3$ crystal (type I). The up-converted fluorescence light was passed through UV band-path filters, a diaphragm, and a monochromator (P250, Nikon) and finally detected by a photomultiplier tube (R585S, Hamamatsu) connected to a photon counter (C5410, Hamamatsu). The spectral width of the fluorescence detected was within ≈4 nm. The signal was sent to a PC which also controlled a stepping motor for an optical delay in the pump arm. The cross correlation trace of the pump and gate pulses had a width (FWHM) of 0.45 ps, and it was used as the instrumental response function (IRF).

The orientation of the $LiIO_3$ crystal was aligned so as to give the maximum cross correlation signal when the polarization of the excitation beam is parallel to that of the gate beam. Fluorescence decay curves were recorded with the polarization of the excitation pulse parallel, perpendicular to or at the magic angle (≈55°) relative to that of the gate pulse to obtain $I_{para}(t)$, $I_{perp}(t)$, and $I_{iso}(t)$. Isotropic fluorescence, $I_{iso}(t)$, was recorded by translating the delay stage to a longer delay (forward scan) and to a shorter delay (backward scan) in every other scan. For anisotropy measurements, parallel ($I_{para}(t)$) or perpendicular ($I_{perp}(t)$) data were collected in every other scan (only forward scan was used). We verified that the initial anisotropy of DMOTCI (3,3′-dimethyloxatricarbocyanine iodide) in ethanol is 0.4 (±0.02) and that the measured magic angle kinetics coincides exactly with that calculated from parallel and perpendicular polarization kinetics. The $t = 0$ in the data was defined at a delay point where the cross-correlation intensity is maximum. The typical peak count from the PS I RC sample was 10−40/s superimposed on a constant background noise (0−1/s). Replacement of the sample with distilled water did not give any noticeable cross correlation trace around $t = 0$ when the other experimental conditions are the same. The exposure time of sample solution (≈0.5 mL) to the excitation laser beam was at most 3 h. After each measurement, we confirmed that the peak position and height of the Q_y band of the sample changed by at most 0.5 nm (blue shift) and 3%, respectively.

3. Results

To avoid ambiguity, we define the usage of the terms "time constant", "rate constant" and "intrinsic rate constant" in the following way. The term time constant is used to refer to the exponential decay times ($t_{1/e}$) obtained directly from experimental data by curve fittings. In contrast, the term rate constant is used to refer to the rate constant of a specific electron or energy transfer between the two states. The term intrinsic rate constant is exclusively used to refer to the rate constant of the primary charge separation from P700* in this paper.

The fluorescence from P700-enriched RC was measured under the P700-neutral conditions. Figure 2a shows polarization-dependent fluorescence decay dynamics observed at 749 nm ($I_{para}(t)$ and $I_{perp}(t)$) upon selective excitation of P700 at 701 nm (the center of the laser spectrum, Figure 1). Fitting the two series of data ($t > 0.25$ ps) independently to convolution of double-exponential curves with the instrument response function (IRF: cross-correlation function) yields the parameters detailed in Table 1. Two time constants ($t_{1/e}$) of 1 and 12−14 ps are obtained. The 1-ps component is much more evident in the parallel kinetics than in the perpendicular one. The time

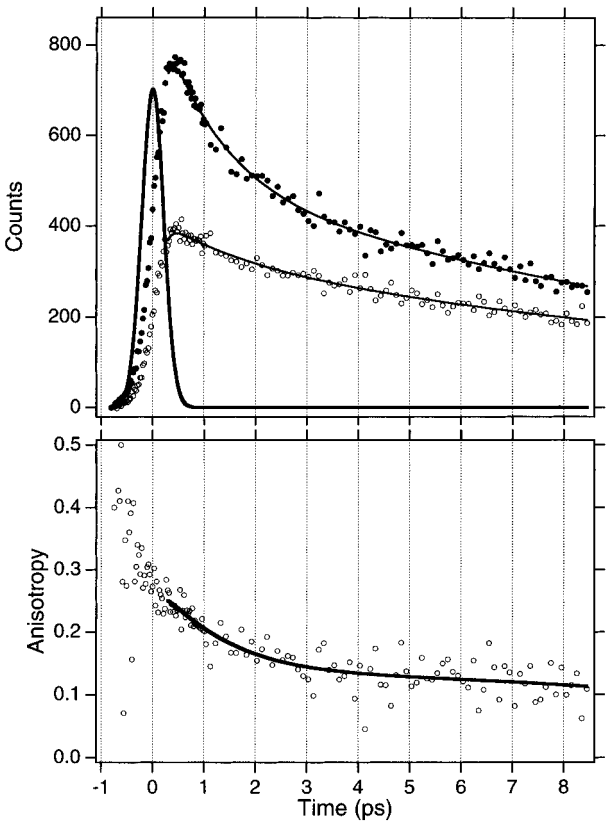

Figure 2. Polarization-dependent fluorescence decays of P700-enriched reaction center upon selective excitation of P700. The sample was excited at 701 nm, and the fluorescence was detected at 749 nm. (a, top) Fluorescence parallel (closed circles) and perpendicular (open circles) to the excitation polarization. Data shown are the sum of 20 scans of each polarization. The instrumental response function (IRF) is shown by the pulselike trace at ≈0 ps. The data are fitted to convolution of the IRF with double-exponential curves (lines). (b, bottom) Raw experimental anisotropy (dots) calculated from the data in (a), and the same function (line) derived from the convoluted fits to the data in a.

dependent anisotropy is defined by

$$r(t) = \frac{I_{\text{para}}(t) - I_{\text{perp}}(t)}{I_{\text{para}}(t) + 2I_{\text{perp}}(t)} \quad (1)$$

Figure 2b shows *r(t)* by the dots. The experimental anisotropy at $t = 0$ ps (at the delay time which gives the maximum cross-correlation intensity) is significantly smaller than 0.4, but it seems to be extrapolated to be above 0.3 in the time region earlier than $t = 0$ ps. The anisotropy is also derived from the fitted parallel and perpendicular curves of Figure 2a and shown by a line in Figure 2b. One can estimate the theoretical initial anisotropy at $t = 0$ ps to be 0.28(±0.02) by using the parameters obtained by the curve fitting in Figure 2a. These results suggest that even double-exponential decay functions with 1- and 12−14-ps time constants do not fit the parallel and perpendicular data sufficiently at the earliest times and that there is an extra fast component ($t_{1/e} < 0.3$ ps: within our time-resolution) causing the initial drop of the anisotropy from 0.4 to ≈0.3.[42] Scans on a longer time scale revealed that a residual anisotropy was ≈0.12 up to 30 ps (the longest time measured).

Figure 3 shows isotropic fluorescence decay observed with the magic angle setup at 749 nm on a 30-ps time scale. Fitting the data ($t > 0.25$ ps) to a sum of two exponentials plus an offset gives lifetimes of 2.2(±0.3) ps and 15.0(±2.9) ps (Figure 3a and Table 1). An attempt to fit the data ($t > 0.25$ ps) to a sum of a single-exponential curve plus an offset is shown in Figure 3b, and this gives a lifetime of 7.4(±0.3) ps (Table 1). Since the residuals for the single-exponential fit are not symmetrically distributed with respect to the zero line, it is evident that at least two exponentials are necessary for the fitting.

Sensitivity of the fitting parameters to the excitation and/or detection wavelengths was also examined. The double-exponential fitting is also necessary for all the other data sets (data not shown) with the other combination of excitation (694 or 701 nm) and detection wavelengths (743, 749, or 760 nm) (Figure 1). In these cases, the time constants obtained on the 30-ps time scale are within the following ranges: 2.2(±1.1)-ps component with 35(±7)% contribution, 15.0(±3.5)-ps one with 55(±7)% and an offset of 10(±5)% of the total signal amplitude.

4. Discussion

4.1. Excitation Equilibration and Charge Separation upon Selective Excitation of P700. The relative amplitude of the 1-ps component is much larger in the parallel kinetics (≈40%) than in the perpendicular one (≈10%) (Figure 2a and Table 1). The difference is responsible for the anisotropy decay from ≈0.3 to ≈0.15 (Figure 2b), which suggests equilibration of excitation energy starting from P700*. One also recognizes an initial drop of the anisotropy from ≈0.4 to ≈0.3 (Figure 2(b)) within the IRF, and this suggests presence of excitation transfer with a time constant of less than ≈0.3 ps.[28] The anisotropy change at times later than 3 ps amounts to at most ≈0.05. The equilibration of excitation energy seems to be substantially complete within 3 ps upon selective excitation of P700.

There are at least two components (2.2 and 15 ps) in the isotropic fluorescence decay on the 30-ps time scale (Figure 3). Given the significant equilibration of excitation energy with a time constant of ≈1 ps, the 15-ps component is attributed to the charge separation from the equilibrated excited state of the RC. The 2.2-ps component is also associated with the charge separation as interpreted below. The previous transient absorption studies have shown that the apparent primary charge separation proceeds with a time constant of 6.5(±1.0) ps.[11,43] A single-exponential fit to the isotropic fluorescence decay in Figure 3b gives 7.4(±0.3) ps (Table 1), which is in fair agreement with the 6.5(±1.0)-ps time constant. This suggests that not only the 15.0-ps component but also a significant portion of the 2.2-ps component should contribute to the overall primary charge separation. Due to a relatively poor signal-to-noise ratio in the rise of transient absorption by $P700^+A_0^-$, it should be as yet difficult to separate the rise of $P700^+A_0^-$ into two components (Table 1).[11] Since the 2.2-ps time constant is comparable to the equilibration time scale (≈1 ps), the 2.2-ps isotropic decay is ascribed to both the excitation equilibration and the primary charge separation before full equilibration of excitation energy.[44] However, the 2.2-ps component does not necessarily give the intrinsic rate constant of the charge separation from P700*. It is necessary to construct a kinetic model which reproduces all the experimental results in order to predict the rate constants associated with the individual process. Analysis based on a kinetic model will be presented in section 4.2.

The fluorescence which did not decay at 30 ps (≈10% of the total amplitude) could be attributed to the charge recombination fluorescence, which has a lifetime of 40−50 ns in the absence of phylloquinone.[40,45] This may also be attributed to chlorophylls with which P700 exchanges excitation energy very slowly. The difference between the absorption spectrum and the excitation spectrum of time-integrated Chl fluorescence at

TABLE 1: Time Constants for the Spontaneous Emission and Transient Absorption of P700-Enriched PSI RC under the P700-Neutral Conditions, along with Excitation (λ_{ex}) and Detection Wavelengths (λ_{det})[a]

	single exp, ps	double exp, ps	λ_{ex}, nm	λ_{det}, nm
parallel fluorescence (9 ps time scale)		1.0(±0.2) (≈40%) 14.3(±2.7)	701	749
orthogonal fluorescence (9 ps time scale)		1.2 (±0.6) (≈10%) 12.3(±6.0)	701	749
magic angle fluorescence (30 ps time scale)	7.4(±0.3) (78%)	2.2(±0.3) (35%) 15.0(±2.9) (55%)	701	749
rise of $P700^+A_0^-$ (30-ps time scale)	6.5(±1.0)[b]		638	740

[a] Error ranges and amplitudes for the lifetimes are shown in the first and second parentheses, respectively. [b] This time constant was obtained by transient absorption spectroscopy in ref 11.

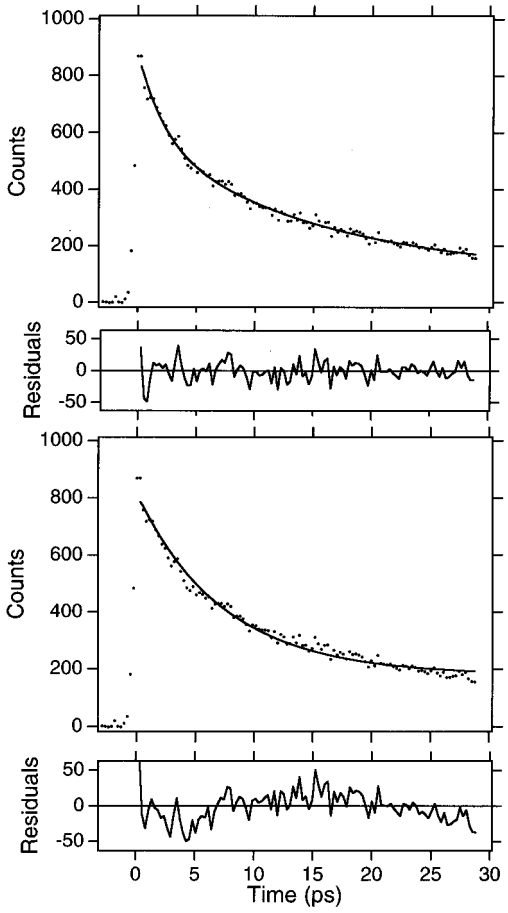

Figure 3. Isotropic fluorescence decay detected at 749 nm upon excitation at 701 nm. Data shown are the sum of 40 scans at the magic angle polarization. (a, top) Data (dots) and a convoluted curve of double-exponential function with the instrumental response function (line). (b, bottom) Data (dots) and a convoluted curve of single-exponential function with the instrumental response function (line). Residuals are the differences between the fitted curves and the data and are shown below each graph.

77 K[36] suggests that some Chls are relatively isolated from P700 in terms of energy transfer. Such Chls may give the long-lived fluorescence. The distinction between the two mechanisms is not yet clear in the present limited time window.

The distribution of excitation energy over different Chl spectral forms upon excitation at 638 nm of the P700-enriched PS I RC was investigated by transient absorption spectroscopy.[11] After subtraction of $P700^+A_0^-$/$P700A_0$ difference spectra from the original transient spectra, the remaining negative absorbance changes between ≈665 and ≈695 nm were attributed mainly to excited Chls (photobleaching plus stimulated emission: PB/SE). The amplitude of the PB/SE spectrum decayed with a ≈9 ps time constant. However, the PB/SE spectral shape remained to be essentially the same and peaked at 681(±2) nm from 0.5 to 13 ps, while the apparent primary charge separation proceeded with a time constant of 6.5 ps.[11] It was thus suggested that excitation energy remains to be distributed over a wide range of Chl spectral forms, especially on Chls absorbing around 681 nm or at shorter wavelength (if contribution of the stimulated emission is taken into account) until the primary charge separation is complete. These Chls are the candidates for the excitation energy acceptor from P700*.

4.2. Kinetic Model. The purpose of this section is to propose a kinetic model as simple as possible but sufficient to qualitatively reproduce the following results. The fast depolarization in the time region earlier than ≈0.3 ps (Figure 2b) suggests that P700 transfers excitation to other chlorophylls on this time scale. Some chlorophylls and P700 exchange excitation with an apparent time constant of ≈1 ps (Figure 2b). Isotropic fluorescence decay shows two time constants of 2.2 and 15 ps (Figure 3a), which correspond to decay of excitation due to the primary charge separation. It is probably reasonable to claim that we have found approximately three time constants: <0.3 ps, 1−2 ps, and 15 ps. At least four states are required in order to reproduce the three exponential time constants.[46] The following four-state model is not unique but is a possible model with necessary and sufficient number of parameters:

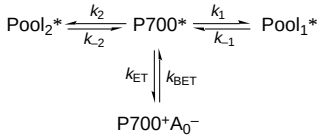

where $Pool_n$* ($n = 1, 2$) are assumed to be ensembles of Chl excited states over which excitation energy can spread upon excitation of P700 on different time scales. There is an alternative model in which $Pool_2$* is connected directly with $Pool_1$* but by relatively small rate constants. Such a case is not considered here. Though we cannot yet specify the spectral identity of $Pool_1$* and $Pool_2$*, they should mainly include the Chls absorbing at ≈681 nm or at shorter wavelengths, as discussed in section 4.1. Excitation exchange between $Pool_1$* and P700* is assumed to be faster than that between $Pool_2$* and P700*. The excitation transfer on a subpicosecond time scale ($t_{1/e}$ < 0.3 ps), which is mainly responsible for the initial drop of anisotropy from 0.4 to ≈0.3 (Figure 2b), is represented mainly by the excitation exchange between P700* and $Pool_1$*. The excitation exchange between $Pool_2$* and P700 mainly gives the ≈1-ps component in the anisotropy decay. The back electron transfer is introduced (by k_{BET}) to reproduce the fluorescence which did not decay at 30 ps (Figure 3).

A set of rate constants for the individual processes which reproduces the fluorescence kinetics should be found. In general, the population changes of the four-state model are represented by triple-exponential functions (see Appendix). We will select rate constants to reproduce three time constants of

≈0.2, 1−2, and ≈15 ps. The 0.2- and 1−2-ps time constants approximately correspond to the ones in the anisotropy decay (<0.3 and 1 ps) and the 1−2- and 15-ps time constants to the ones in the isotropic decay (2.2 and 15 ps) (Table 1). It is not easy to exactly satisfy the imposed conditions, but the following set of rate constants approximately meet the requirements:

$$(k_1, k_{-1}, k_2, k_{-2}, k_{ET}, k_{BET}) = (2.5, 2.5, 0.5, 0.15, 0.5, 0.008\ \mathrm{ps}^{-1}) \quad (2)$$

The selection of these parameters will be described later in this section. Given eq 2 and the following initial conditions,

$$[\mathrm{P700}^*] = 1 \quad \text{at} \quad t = 0 \quad (3)$$

the time-dependent population of each state is represented by (see Appendix)

$$\begin{bmatrix} [\mathrm{P700}^*] \\ [\mathrm{Pool}_1{}^*] \\ [\mathrm{Pool}_2{}^*] \\ [\mathrm{P700}^+\mathrm{A}_0{}^-] \end{bmatrix} = k\nu_1 \exp(-t/0.18) + k\nu_2 \exp(-t/1.9) + k\nu_3 \exp(-t/14.5) + k\nu_4 \quad (4)$$

where

$$k\nu_1 = \begin{bmatrix} 0.598 \\ -0.489 \\ -0.055 \\ -0.054 \end{bmatrix} \quad (5)$$

$$k\nu_2 = \begin{bmatrix} 0.318 \\ 0.408 \\ -0.417 \\ -0.304 \end{bmatrix} \quad (6)$$

$$k\nu_3 = \begin{bmatrix} 0.068 \\ 0.070 \\ 0.422 \\ -0.560 \end{bmatrix} \quad (7)$$

$$k\nu_4 = \begin{bmatrix} 0.015 \\ 0.015 \\ 0.051 \\ -0.918 \end{bmatrix} \quad (8)$$

The elements in $k\nu_n$ ($n = 1-4$) with positive and negative signs indicate decaying and rising populations, respectively. The fluorescence decays at 749 nm under all the polarization conditions (parallel, perpendicular, and magic angle) are represented by the time constants of 0.18, 1.9, and 14.5 ps (eq 4). The first term in eq 4, $k\nu_1 \exp(-t/0.18)$, is mainly associated with the excitation exchange between P700* and Pool_1* ([P700*] decays, and [Pool_1*] rises). The second term in eq 4, $k\nu_2 \exp(-t/1.9)$, is associated with the excitation exchange among P700*, Pool_1*, and Pool_2 and also with the primary charge separation ([P700*] and [Pool_1*] decay, but [Pool_2*] and [$\mathrm{P700}^+\mathrm{A}_0{}^-$] rise). The third term in eq 4, $k\nu_3 \exp(-t/14.4)$, is associated with the decay of the whole excited states (all the excited states, [P700*], [Pool_1*], and [Pool_1*] decay, and [$\mathrm{P700}^+\mathrm{A}_0{}^-$] rises).

The isotropic fluorescence intensity at 749 nm, $F_{\mathrm{magic},749}$, is assumed to be given by

$$F_{\mathrm{magic},749} = [\mathrm{P700}^*] + [\mathrm{Pool}_1{}^*] + [\mathrm{Pool}_2{}^*] \quad (9)$$

Convolution of $F_{\mathrm{magic},749}$ with the experimental IRF is shown in Figure 4a. A double-exponential function is forced to fit the simulated decay in the time region after the peak of the signal. Two exponential components of 1.9 ps (33%) and 14.4 ps (59%) were obtained (fitted curve not shown). Parallel and perpendicular fluorescence were simulated by

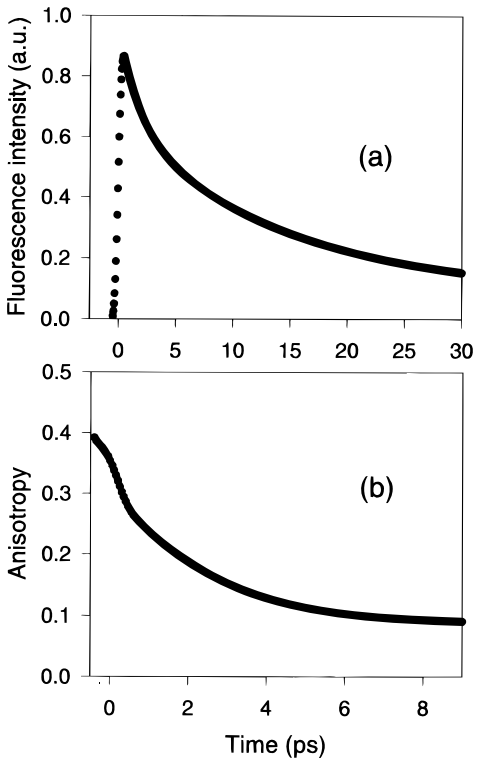

Figure 4. Simulated isotropic fluorescence decay (a) and anisotropy function (b) upon selective excitation of P700 in the four-state model (see section 4.2). The rate constants used are shown in eq 2. The isotropic decay is defined as the total population of the excited states (eq 9). For the anisotropy function, the angles between transition dipole moments are assumed to be 30° between P700* and Pool_1* and 55° between P700* and Pool_2*. See section 4.2 for the details.

$$I_{\mathrm{para}}^{\mathrm{sim}}(t) = \frac{1}{5}\{[\mathrm{P700}^*]3 + [\mathrm{Pool}_1{}^*](1 + 2\cos^2\theta_1) + [\mathrm{Pool}_2{}^*](1 + 2\cos^2\theta_2)\} \quad (10)$$

and

$$I_{\mathrm{perp}}^{\mathrm{sim}}(t) = \frac{1}{5}\{[\mathrm{P700}^*]1 + [\mathrm{Pool}_1{}^*](1 + \sin^2\theta_1) + [\mathrm{Pool}_2{}^*](1 + \sin^2\theta_2)\} \quad (11)$$

The convolutions of the simulated parallel (eq 10) and perpendicular (eq 11) fluorescence intensities with IRF are calculated separately, and the two convoluted curves were used to obtain the anisotropy decay by using eq 1 (Figure 4b). The angles between the transition dipole moments of P700* and Pool_1* ($\theta_1 = 30°$) and of P700* and Pool_2* ($\theta_2 = 55°$) were determined by fitting the simulated anisotropy to the experimental one in Figure 2b. These simulated curves (Figure 4) show features in fair agreement with those of the fluorescence up-conversion data (Figures 2 and 3).

Selection of the set of rate constants shown as eq 2 is now considered. The ratio between k_2 and k_{-2} was adjusted in order to make a proper ratio between the second and the third shortest time constants (the 1.9- and 14.5-ps time constants in eq 4). The value of k_2 should be approximately equal to k_{ET} in order for the double-exponential feature in the time region later than 1 ps to be clear. The ratio between k_1 and k_{-1} values cannot

be determined uniquely by experiments but was determined so that the [P700*] at the equilibrium (P^e_{P700}) is in good agreement with the one given by the Boltzmann equilibrium. P^e_{P700} at the Boltzmann equilibrium (at 278 K) is estimated to be 0.2−0.3,[47] when the spectral decomposition of the absorption spectrum in Figure 1 is used and all the pigments are included.[11] In the above simulation with $k_1 \approx k_{-1}$, P^e_{P700} is ≈0.3 at 3 ps (pseudoequilibrium among the excited states, cf. eq A.10b) and ≈0.2 at 30 ps (equilibrium among excited states and the charge separated state, cf. eq A.10c). In summary, the following relationship should be satisfied:

$$k_1 \approx k_{-1} \gg k_2 \approx k_{ET} > k_{-2} \gg k_{BET} \qquad (12)$$

This indicates that rate constant of some excitation-transfer step is comparable to or smaller than the intrinsic rate constant of the electron transfer from P700*.

Finally, the intrinsic rate constant of the primary electron transfer used above ($k_{ET} = 0.5$ ps^{-1} in eq 2) is compared with the predicted rate constant for RCs with more antenna Chls. It is comparable to the ones in refs 3, 27, and 48 (0.25−0.6 ps^{-1}), but substantially smaller than the one in ref 31 (2.3 ps^{-1}). The k_{ET} value to reproduce experimental time constants is sensitive to the ratio between k_2 and k_{-2} and also to the one between k_1 and k_{-1}. The former was approximately determined by the experimental results, but the latter was determined by assuming the Boltzmann equilibrium among all the Chls in the RC particle (see the previous paragraph). This assumption is not necessarily valid because some Chls in the present RC particle are relatively isolated from P700 in terms of excitation exchange. A lower limit for k_{ET} is given when k_1 is substantially smaller than k_{-1}. This condition results in a higher probability of P700 excitation and smaller optimized k_{ET} to reproduce the experimental time constants. The k_{ET} is thus shown to be at least 0.25 ps^{-1}.

4.3. Comparison of the Present Results with Other Studies. The fluorescence depolarization in this study is different from those observed by Du *et al*., who observed 150−300-fs single-exponential decay of fluorescence anisotropy from ≈0.34 to 0.1−0.2 in PS I RC samples (≈40 Chl/P700) from *Chlamydomonas reinhardtii*.[28] They associated this time with single-step energy transfer,[28] which is supported by simulations.[27,30] Since the antenna size of the RC preparations in ref 28 was relatively large (≈40 Chl/P700), different Chls are probably excited in different RC units by the employed wavelengths (630−656 nm). Single-step energy transfers from P700 could also proceed with 0.15−0.3-ps time constants in the present particles, which results in only a partial depolarization from the initial anisotropy of 0.4 to ≈0.3. The remaining anisotropy decay from ≈0.3 to ≈0.15 is associated with the 1-ps excitation equilibration. These may indicate that the angles between the Q_y transition dipole moments of P700 and its nearest-neighbor Chls are smaller than the average one between those of other nearest-neighbor Chl pairs.

The time scale of full excitation equilibration (≈1 ps) is somewhat shorter than those estimated on PS I RCs retaining more antenna Chls.[5,9] Hastings *et al.* have studied excitation-wavelength dependence of the equilibration dynamics in a photosystem II deletion mutant of *Synechocystis* sp. PCC6803 (≈100 Chl/P700).[5] The equilibration time constant was in the 2.7−4.3-ps range.[5] This time constant is in good agreement with the one (3.3−6.6 ps) obtained by Struve *et al*. on PS I RC with ≈60 antenna Chls[32,34] and the one (5 ps) by Du *et al.* on PS I RC with ≈40 antenna Chls.[28] Even longer equilibration time constants of 7−12 ps on PS I RC particles from *Synechococcus* sp. are reported by Holzwarth *et al.*,[9] which, however, may reflect the significantly increased number of long-wavelength-absorbing Chls.[5] The relatively short time constant in this study should reflect the extraction of most of the antenna Chls and/or the local environment of P700. There are two possible explanations. Firstly, the extraction of most of the antenna Chls may result in a situation where excitation can migrate only in the vicinity of P700 upon excitation of P700 and the equilibration time in the vicinity of P700 is short. Secondly, all the Chls retained in the present particles may be spatially localized compared with the full extension of the antenna Chls in the other RC preparations, which enables relatively rapid excitation exchange among the Chls. However, proper explanation should await for further systematic comparison between different RC preparations.

The residual anisotropy at 9 ps or later times (≈0.12, Figure 2b) is also observed in RC with more antenna Chls.[28,29,32−34] This reflects the relative orientation of Chl molecules in PS I RC particles.[19,20,32−34,49] The average transition dipole moment of the residual fluorescence (Figure 3) is estimated to be tilted by ≈40° relative to that of P700 (Figure 2b) by using the following equation:

$$r(t) = \frac{1}{5}(3\cos^2\Theta(t) - 1) \qquad (13)$$

$\Theta(t)$ is the angle between transition dipole moments of absorption and fluorescence. In linear dichroism measurements on P700-enriched RCs (≈10 Chl/P700), Chl forms absorbing at 670−675 nm were estimated to have Q_y (0−0) transitions tilted by 40°(±5°) relative to that of P700.[50] Considering extensive distribution of excitation energy to Chl forms absorbing at 681 nm or at shorter wavelength (see the last paragraph in section 4.1.),[11] the coincidence of the above two angles (obtained by fluorescence anisotropy and linear dichroism) may be reasonable.

5. Concluding Remarks

The primary electron transfer and excitation transfer starting from a selectively excited P700 are observed for the first time in PS I RC with ≈14 Chls per P700. Energetically uphill excitation transfers from P700* to shorter-wavelength-absorbing Chl forms lead the excited Chls to decay with at least two time constants of ≈2 and ≈15 ps. The fast and slow components indicate the charge separation before and after full equilibration of excitation energy, respectively. The depolarization of fluorescence in this study (mainly with ≈1-ps time constant) is not complete on the time scale of single-step excitation transfer[28] but somewhat faster than excitation equilibration in PS I RCs with more antenna Chls (>40 Chls/P700).[3,5−9,28,29,32−34] Kinetic features of the fluorescence data are reasonably reproduced by the four-state model, which shows that the intrinsic rate constant of the electron transfer from P700* is > 0.25 ps^{-1}.

Acknowledgment. We thank Prof. S. Itoh, Prof. M. Mimuro, and Dr. M. Iwaki for giving us spectral decomposition data on P700-enriched preparations and for their invaluable suggestions, Drs. D. M. Joseph, Y. Nagasawa, K. Tominaga, M. Du, Y. Jia, D. R. Klug, J. R. Durrant, and C. J. Barnett for their advice on the experimental setup, and Mr. S. Katoh for making the excellent sample spinner and the cells. This work was supported in part by the New Energy and Industrial Technology Development Organization (NEDO).

Appendix

The time-dependent population change of the four-state model in section 4.2. is solved by the so-called determinant method[46] as follows.

The differential equation is

$$\frac{d\boldsymbol{x}(t)}{dt} = \boldsymbol{M}(k_1,k_{-1},k_2,k_{-2},k_{ET},k_{BET})\boldsymbol{x}(t) \qquad (A.1)$$

where

$$\boldsymbol{M}(k_1,k_{-1},k_2,k_{-2},k_{ET},k_{BET}) = \begin{bmatrix} -k_1 & -k_2 - k_{ET} & k_{-1} & k_{-2} & k_{BET} \\ & k_1 & -k_{-1} & 0 & 0 \\ & k_2 & 0 & -k_{-2} & 0 \\ & k_{ET} & 0 & 0 & -k_{BET} \end{bmatrix} \qquad (A.2)$$

and

$$\boldsymbol{x}(t) = \begin{bmatrix} [P700^*] \\ [Pool_1^*] \\ [Pool_2^*] \\ [P700^+A_0^-] \end{bmatrix} \qquad (A.3)$$

Given the four eigenvalues of $\boldsymbol{M}(k_1,k_{-1},k_2,k_{-2},k_{ET},k_{BET})$ ($-\lambda_1$, $-\lambda_2$, $-\lambda_3$, $-\lambda_4$) and the four corresponding eigenvectors ($\boldsymbol{p}_1$, $\boldsymbol{p}_2$, $\boldsymbol{p}_3$, $\boldsymbol{p}_4$), $\boldsymbol{x}(t)$ can be solved:

$$\boldsymbol{x}(t) = \boldsymbol{P}\exp(\boldsymbol{\Lambda}t)\,\boldsymbol{P}^{-1}\boldsymbol{x}(0) \qquad (A.4)$$

where

$$\boldsymbol{P} = [\boldsymbol{p}_1,\boldsymbol{p}_2,\boldsymbol{p}_3,\boldsymbol{p}_4] \qquad (A.5)$$

$$\boldsymbol{\Lambda} = \begin{bmatrix} -\lambda_1 & 0 & 0 & 0 \\ 0 & -\lambda_2 & 0 & 0 \\ 0 & 0 & -\lambda_3 & 0 \\ 0 & 0 & 0 & -\lambda_4 \end{bmatrix} \qquad (A.6)$$

A set of vectors $k\nu_n$ ($n = 1-4$) is defined as follows:

$$k\nu_n = \boldsymbol{P}\boldsymbol{E}_n\boldsymbol{P}^{-1}x(0) \qquad (A.7)$$

where $\boldsymbol{E}_n$ is the matrix with only one nonzero element of 1 as the nth diagonal element.

For example,

$$\boldsymbol{E}_1 = \begin{bmatrix} 1 & 0 & 0 & 0 \\ 0 & 0 & 0 & 0 \\ 0 & 0 & 0 & 0 \\ 0 & 0 & 0 & 0 \end{bmatrix} \qquad (A.8)$$

The solution (A.4) can be rewritten as

$$\boldsymbol{x}(t) = \sum_n k\nu_n \exp(-\lambda_n t) \qquad (A.9)$$

This type of expression is used in section 4.2. Given the set of rate constants by eq 2, $\boldsymbol{x}(t)$'s at representative times (ps) are shown as follows:

$$\boldsymbol{x}(0.5) = \begin{bmatrix} 0.363 \\ 0.363 \\ 0.134 \\ 0.140 \end{bmatrix} \qquad (A.10a)$$

$$\boldsymbol{x}(3.0) = \begin{bmatrix} 0.136 \\ 0.156 \\ 0.308 \\ 0.400 \end{bmatrix} \qquad (A.10b)$$

$$\boldsymbol{x}(12.0) = \begin{bmatrix} 0.024 \\ 0.024 \\ 0.104 \\ 0.848 \end{bmatrix} \qquad (A.10c)$$

References and Notes

(1) Wasielewski, M. R.; Fenton, J. M.; Govindjee, T. *Photosynth. Res.* **1987**, *12*, 181.

(2) Klug, D. R.; Giorgi, L. B.; Crystal, B.; Barber, J.; Porter, G. *Photosynth. Res.* **1989**, *22*, 277.

(3) Hastings, G.; Kleinherenbrink, F. A. M.; Lin, S.; Blankenship, R. E. *Biochemistry* **1994**, *33*, 3185.

(4) Hastings, G.; Kleinherenbrink, F. A. M.; Lin, S.; McHugh, T. J.; Blankenship, R. E. *Biochemistry* **1994**, *33*, 3193.

(5) Hastings, G.; Reed, L. J.; Lin, S.; Balnkenship, R. E. *Biophys. J.* **1995**, *69*, 2044.

(6) Hastings, G.; Hoshina, S.; Webber, A. N.; Blankenship, R. E. *Biochemistry* **1995**, *34*, 15512.

(7) Turconi, S.; Schweitzer, G.; Holzwarth, A. R. *Photochem. Photobiol.* **1993**, *57*, 113.

(8) Turconi, S.; Weber, N.; Schweitzer, G.; Holzwarth, A. R. *Biochim. Biophys. Acta* **1994**, *1187*, 324.

(9) Holzwarth, A. R.; Schatz, G. H.; Brock, H.; Bittermann, E. *Biophys, J.* **1993**, *64*, 1813.

(10) Kumazaki, S.; Iwaki, M.; Ikegami, I.; Kandori, H.; Yoshihara, K.; Itoh, S. *J. Phys. Chem.* **1994**, *98*, 11220.

(11) Kumazaki, S.; Kandori, H.; Petek, H.; Yoshihara, K.; Ikegami, I. *J. Phys. Chem.* **1994**, *98*, 10335.

(12) Kamogawa, K.; Morris, J. M.; Takagi, Y.; Nakashima, N.; Yoshihara, K.; Ikegami, I. *Photochem. Photobiol.* **1983**, *37*, 207.

(13) Kim, D.; Yoshihara, K.; Ikegami, I. *Plant Cell Physiol.* **1989**, *30*, 679.

(14) Iwaki, M.; Kumazaki, S.; Yoshihara, K.; Erabi, T.; Itoh, S. *J. Phys. Chem.* **1996,** *100*, 10802.

(15) Shuvalov, V. A.; Nuijis, A. M.; van Gorkom, H. J.; Smit, H. W. J.; Duysens, L. N. M. *Biochim. Biophys. Acta* **1986**, *850*, 319.

(16) Brettel, K.; *FEBS Lett.* **1988**, *239*, 246.

(17) Evans, M. C. W.; Nugent, J. H. A. In *The Photosynthetic Reaction Center;* Deisenhofer, J., Norris, J. R., Eds.; Academic: London, 1993; Vol. 1, p 391.

(18) White, N. T. H.; Beddard, G. S.; Throne, J. R. G.; Feehan, T. M.; Keyes, T. E.; Heathcote, P. *J. Phys. Chem.* **1996**, *100*, 12086.

(19) Krauss, N.; Schubert, W.-D.; Klukas, O.; Fromme, P.; Witt, H. T.; Saenger, W. *Nat. Struct. Biol.* **1996**, *3*, 965.

(20) Krauss, N.; Hinrichs, W.; Witt, I.; Fromme, P.; Pritzkow, W.; Dauter, Z.; Betzel, C.; Wilson, K. S.; Witt, H. T.; Saenger, W. *Nature* **1993**, *361*, 326.

(21) Deisenhofer, J.; Michel, H. *EMBO J.* **1989**, *8*, 2149.

(22) Allen, J. P.; Feher, G.; Yeats, T. O.; Komiya, H.; Rees, D. C. *Proc. Natl. Acad. Sci. U.S.A.* **1987**, *84*, 5730.

(23) Van Grondelle, R.; Dekker, J. P.; Gillbro, T.; Sundstrom, V. *Biochim. Biophys. Acta* **1994**, *1187*, 1.

(24) Van der Lee, J.; Bald, D.; Kwa, S. L. S.; Van Grondelle, R.; Rögner, M.; Dekker, J.P. *Photosynth. Res.* **1993**, *35*, 311.

(25) Shubin, V. V.; Bezsmertnaya, I. N.; Karapetyan, N. V. *J. Photochem. Photobiol. B* **1995**, *30*, 153.

(26) Werst, M.; Jia, Y.; Mets, L.; Fleming, G. R. *Biophys. J.* **1992**, *61*, 868.

(27) Owens, T. G.; Webb, S. P.; Mets, L.; Alberte, R. S.; Fleming, G. R. *Proc. Natl. Acad. Sci. U.S.A.* **1987**, *84*, 1532.

(28) Du, M.; Xie, X.; Jia, Y.; Mets, L.; Fleming, G. R. *Chem. Phys. Lett.* **1993**, *201*, 535.

(29) Lin, S.; Van Amerongen, H.; Struve, W. S. *Biochim. Biophys. Acta* **1992**, *1140*, 6.

(30) Jia, Y.; Jean, J. M.; Werst, M. M.; Chan, C.-K.; Fleming, G. R. *Biophys. J.* **1992**, *63*, 259.

(31) Trinkunas, G.; Holzwarth, A. R. *Biophys. J.* **1994**, *66*, 415.

(32) Causgrove, T. P.; Yang, S.; Struve, W. S. *J. Phys. Chem.* **1988**, *92*, 6121.

(33) Causgrove, T. P.; Yang, S.; Struve, W. S. *J. Phys. Chem.* **1989**, *93*, 6844.

(34) Struve, W. S. *J. Opt. Soc. Am. B* **1990**, *7*, 1586.

(35) Ikegami, I.; Katoh, S. *Biochim. Biophys. Acta* **1975**, *376*, 588.

(36) Iwaki, M.; Mimuro, M.; Itoh, S. *Biochim. Biophys. Acta* **1992**, *1100*, 278.

(37) Ikegami, I.; Itoh, S. *Biochim. Biophys. Acta* **1988**, *934*, 39.

(38) Mimuro, M. *Plant Cell Physiol.* **1993**, *34*, 321.

(39) Mimuro reported a long-wavelength-absorbing Chl spectral form in P700-enriched PS I RC.[38]

(40) Ikegami, I.; Setif, P.; Mathis, P. *Biochim. Biophys. Acta* **1987**, *894*, 414.

(41) About 40% of the whole P700 is estimated to be at the triplet state ($P700^T$) during the measurement by assuming the quantum yield of the generation and lifetime of the $P700^T$ are 0.3 and 70 μs (ref 40), respectively. However, the absorption cross section of RC particles with $P700^T$ should be depleted at the present excitation wavelength (701 nm), where the absorptuion of P700 is dominant. It is thus assumed that the present time-resolved fluorescence results mostly from the RCs which are in the ground state before excitation.

(42) Curve fitting of three-exponential functions with two fixed time constants of 1 and 12−14 ps to the parallel and perpendicular data in the time region between −0.25 and 0.5 ps did not converge properly.

(43) In ref 11, this time constant was determined from the rise of the absorption of $P700^+A_0^-$ at 740(±10) nm upon 638-nm excitation, where absorption changes of Chl excited states are negligible. Even though the measurement in ref 11 was carried out with parallel pump−probe polarization conditions, the rise time of $P700^+A_0^-$ should not depend on the polarization conditions.

(44) There remains a residual equilibration process even after 3 ps, as indicated by the slow anisotropy change with ≈10-ps time constant. Its contribution to the anisotropy change is at most ≈0.05. We regard that the ≈1-ps equilibration process achieves full equilibration of the excited states for simplicity in the following discussion.

(45) Itoh, S.; Iwaki, M. *Biochim. Biophys. Acta* **1988**, *934*, 32.

(46) Steinfeld, J. I.; Francisco, J. S.; Hase, W. L. *Chemical Kinetics and Dynamics*; Prentice-Hall: Englewood Cliffs, NJ, 1989.

(47) This probability is different from that in ref 11, where P^e_{P700} was given by the product of the number of Chl molecules forming P700 (2) and the Boltzmann distribution probability. However, the factor of 2 is not necessary if P700* is one excited state delocalized over two chlorophyll molecules. In this study, P^e_{P700} is assumed to be about half that estimated in ref 11.

(48) Trissl, H.-W.; Hecks, B.; Wulf, K. *Photochem. Photobiol.* **1993**, *57*, 108.

(49) Haworth, P.; Tapie, P.; Arntzen, J.; Breton, J. *Biochim. Biophys. Acta* **1982**, *682*, 152.

(50) Breton, J.; Ikegami, I. *Photosynth. Res.* **1989**, *21*, 27.

(51) This set of spectral decomposition data was obtained by Prof. S. Itoh, Prof. M. Mimura, and Dr. M. Iwaki and used here with their permission. See also ref 36.